A Microwave Infrared Threshold Technique to Improve the GOES Precipitation Index

LIMING XU, XIAOGANG GAO, AND SOROOSH SOROOSHIAN

Department of Hydrology and Water Resources, The University of Arizona, Tucson, Arizona

PHILLIP A. ARKIN

International Research Institute for Climate Prediction, Lamont-Doherty Earth Observatory, Palisades, New York

BISHER IMAM

Department of Hydrology and Water Resources, The University of Arizona, Tucson, Arizona

(Manuscript received 26 March 1998, in final form 9 July 1998)

ABSTRACT

A method to improve the GOES Precipitation Index (GPI) technique by combining satellite microwave and infrared (IR) data is proposed and tested. Using microwave-based rainfall estimates, the method, termed the Universally Adjusted GPI (UAGPI), modifies both GPI parameters (i.e., the IR brightness temperature threshold and the mean rain rate) to minimize summation of estimation errors during the microwave sampling periods. With respect to each grid, monthly rainfall estimates are obtained in a manner identical to the GPI except for the use of the optimized parameters. The proposed method is compared with the Adjusted GPI (AGPI) method of Adler et al. (1993), which adjusts the GPI monthly rainfall estimates directly using an adjustment ratio. The two methods are compared using the First Algorithm Intercomparison Project (AIP/1) dataset, which covers two month-long periods over the Japanese islands and surrounding oceanic regions. Two types of microwave-related errors are addressed during the comparison: (1) sampling error caused by insufficient sampling rate and (2) measurement error of instantaneous rain rate. Radar–gauge composite rainfall observations were used to simulate microwave rainfall estimates for studying the sampling error. The results of this comparison show that UAGPI is more capable of utilizing the limited information contained in sparse microwave observations to reduce sampling error and that UAGPI demonstrates stronger resistance to microwave measurement error. Comparison between the two methods using three different sizes of moving-average windows indicates that, while the smoothing operation is crucial to AGPI, it is not essential for UAGPI to consistently perform better than AGPI. This indicates that UAGPI provides stable estimates of monthly rainfall at various spatial scales.

1. Introduction

Recent advances in rainfall estimation from satellite imagery have been driven largely by two interconnected factors. First, there is the lack of ground-based precipitation measurements over most of the earth's surface. The second factor is the ever-increasing demand by global-scale climate, weather, hydrologic, and water resources studies for more accurate, higher resolution, and longer-duration global precipitation datasets. Yet, and because of the weak and rather indirect connection between the physical properties that can be measured by satellites and the actual surface rainfall, there remains a great deal of uncertainty associated with satellite-based rainfall estimates (Arkin and Ardanuy 1989). For example, because of high spatial and temporal resolutions necessary to describe the fast variation of precipitation, infrared (IR) images obtained from geosynchronous satellites are commonly used for rainfall estimation over wide areas. However, geosynchronous satellite IR measurements correspond to cloud-top brightness temperature, which is indirectly related to surface rainfall. On the other hand, microwave signals obtained from polar-orbiting satellites are physically related to the radiation transfer of cloud hydrometeors, but their poor temporal resolution (one or two overpasses per day) provides only sparse ''snapshots'' of precipitation. Clearly, and as mentioned by Adler et al. (1993), there are opportunities to improve precipitation estimates by combining the two types of data so that the strengths of each individual technique are maintained and their weaknesses are compensated for.

The Geostationary Operational Environmental Satellite (GOES) Precipitation Index (GPI) (Arkin and

Corresponding author address: Dr. Soroosh Sorooshian, Department of Hydrology and Water Resources, The University of Arizona, Tucson, AZ 85721-0011.
E-mail: soroosh@hwr.arizona.edu

Meisner 1987) is a simple IR threshold algorithm that utilizes the high sampling rate and spatial resolution of IR observations made by GOES satellites. GPI performed as well as or better than most other techniques in several consecutive algorithm intercomparison projects (Ebert et al. 1996). In addition, GPI was applied to produce tropical and subtropical (40°N–40°S) precipitation products for various climatological studies (Arkin and Xie 1994) and was adopted as the basic IR-based algorithm for the GPCP (Global Precipitation Climatology Project) (Huffman et al. 1997) and the CPC [National Oceanic and Atmospheric Administration (NOAA) Climate Prediction Center] Merged Analysis of Precipitation (Xie and Arkin 1996, 1997). More recently, GPI was selected among the rainfall retrieval algorithms to be tested during the National Aeronautics and Space Administration/earth observing system Tropical Rainfall Measurement Mission (TRMM) program (Huffman et al. 1997; Simpson et al. 1988). Several researchers pointed out that GPI-based rainfall estimates require seasonal and regional adjustments in order to account for the global variability of rainfall regimes (Morrissey and Greene 1993; Arkin and Xie 1994). Such adjustments can be attained either by (a) directly modifying the estimated rainfall or by (b) adjusting the two GPI parameters (i.e., IR brightness temperature threshold and the mean rainfall rate). The most commonly used GPI adjustment method was proposed by Adler et al. (1993). Their approach, which falls under category (a), has been termed the Adjusted GPI (AGPI). It employs a microwave-based adjustment ratio to modify GPI's monthly rainfall estimates. Further details on AGPI are provided in section 2 below. AGPI has been used by the GPCP version 1a Global Precipitation dataset and has been selected as one of the core algorithms to be tested during the TRMM mission (Huffman et al. 1997).

Other data-merging techniques also have been designed to produce rainfall estimates from a combination of various data sources, including IR, microwave, rain gauges, and numerical weather models according to their statistical properties (Huffman et al. 1997). Hsu et al. (1997) and Sorooshian (1997) used microwave rainfall estimates to perform adaptive training for an IR-based Artificial Neural Network model for rainfall estimation. Their results indicate that using partially available microwave data improves the performance of IR-based rainfall estimation both at short-term (daily) and long-term (monthly) cases.

In this paper, we propose a type (b) method, the Universally Adjusted GOES Precipitation Index (UAGPI), to adjust both parameters of the GPI algorithm using microwave data. The main objective of this adjustment is to reduce the uncertainty in GPI rainfall estimates and to allow one to vary its two parameters so that they reflect different rainfall regimes. The ability of both AGPI and UAGPI to extract the most from the limited information on rainfall regimes provided by the sparse sampling rate of microwave data is also examined. The next section is devoted to a brief background description of the relevant IR and microwave techniques used in this study, including GPI, AGPI, and microwave Scattering Index (SI). The UAGPI method is described in section 3, along with an expression of the monthly rainfall error in terms of monthly mean rain rate and rainfall area. In section 4, the First Algorithm Intercomparison Project (AIP/1) dataset (Lee et al. 1991) is used to compare UAGPI and AGPI. The two methods will be evaluated in a grid-based configuration as well as in the moving-average window configuration recommended by Adler et al. (1993). Conclusions and recommendations for future work are presented in section 5.

2. Background

a. The GPI algorithm

Arkin (1979) and Arkin and Meisner (1987) developed an empirical relationship between IR brightness temperature at cloud-top and surface rainfall. The algorithm, originally developed from radar and satellite data collected in the Global Atmospheric Research Program Atlantic Tropical Experiment, uses a fixed IR brightness temperature (235 K) as a threshold to differentiate between rain and no-rain pixels. A fractional rain coverage is calculated as the ratio of the number of cloud pixels colder than 235 K to the number of total pixels in a 2.5° grid square. A constant mean rain rate of 3 mm h^{-1} is assigned to the fractional rain area to obtain the instantaneous rainfall. Finally, the instantaneous rainfall is accumulated to produce monthly rainfall estimates.

b. The AGPI method

Adler et al. (1993) developed the Adjusted GPI (AGPI) algorithm to modify the GPI rainfall estimates using the superior instantaneous rain-rate estimates obtained from microwave techniques. AGPI is based on adjusting rain rate with an adjustment ratio derived from the microwave rainfall estimates. This method provides a means of correcting estimation bias for GPI. Specifically, the adjustment ratio for each grid is given as

$$r_a = \frac{V_M}{V_{\mathrm{MIR}}}, \tag{1}$$

where r_a is the adjustment ratio, V_M is the total monthly rainfall estimate for a grid by a microwave technique, and V_{MIR} is the total monthly rainfall estimations by GPI using the IR data closely coincident with microwave observations.

A monthly rainfall estimate for each grid is then derived by applying the adjustment ratio to GPI estimates calculated with the full hourly IR data. To reduce the effects of unrealistic large variations of r_a when computed for relatively small spatial scales, Adler et al.

(1993) recommended that V_M and V_{MIR} be smoothed before the ratio is computed. Smoothing is attained by using a moving-average window of a 5×5 grid box. They also suggested that the ratio be restricted within the range [0.2–2.0] to prevent unreasonably large departures from unity (Adler et al. 1994).

c. The microwave Scattering Index scheme

In this paper, the SI technique proposed by Ferraro and Marks (1995) is used to compute rain rates from microwave data. In the Ferraro and Marks technique, which is an improvement of the original SI method developed by Grody (1991), an index of rain rate is computed using brightness temperatures derived from three vertically polarized Special Sensor Microwave Imager (SSM/I) channels. These channels are 19.35, 22.235, and 85.5 GHz. Specifically, SI over land (SI_L) and ocean (SI_W) are defined as follows (Ferraro and Marks 1995):

$$\mathrm{SI}_L = 451.9 - 0.44\mathrm{TB}_{19\mathrm{V}} - 1.775\mathrm{TB}_{22\mathrm{V}} + 0.00575\mathrm{TB}_{22\mathrm{V}}^2 - \mathrm{TB}_{85\mathrm{V}} \quad \text{(land)}$$

and

$$\mathrm{SI}_W = -174.4 + 0.72\mathrm{TB}_{19\mathrm{V}} + 2.439\mathrm{TB}_{22\mathrm{V}} - 0.00504\mathrm{TB}_{22\mathrm{V}}^2 - \mathrm{TB}_{85\mathrm{V}} \quad \text{(water)},$$

where TB denotes brightness temperature (K), and the subscripts indicate the SSM/I channels. Once an SI value is computed, a minimum threshold of 10 K is used to differentiate rain and no-rain pixels. For rain pixels, rain rates are computed as follows:

$$R_L = 0.0257\mathrm{SI}_L^{1.734} \quad \text{(land)}$$

and

$$R_W = 0.0012\mathrm{SI}_W^{2.168} \quad \text{(water)}.$$

The coefficients of these equations were calibrated by Ferraro and Marks (1995) with the AIP/1 dataset described later.

3. Description of the Universally Adjusted GPI

Within each grid square, UAGPI is conceptually based on the selection of the two GPI parameters for a given month so that a measure of the total error between IR-based and observed rainfall estimates is minimized (Xu 1997). Because climate studies commonly require fields of monthly precipitation at scales ranging from $1^\circ \times 1^\circ$ to $2.5^\circ \times 2.5^\circ$, an appropriate calibration objective function is the error in estimating the total monthly rainfall for a comparable grid scale. Let R be the observed number of hourly rain pixels in a grid over a given month, and define N as the estimated value of R. Then, the error of monthly rainfall estimation for the grid is written as follows:

$$E = V^e - V^o = (\overline{p}^e N - \overline{p}^o R)/K, \tag{2}$$

where V^e is the estimated monthly total rainfall depth (mm), V^o is the observed monthly total rainfall depth (mm), $\overline{p}^e$ is the estimated mean pixel rain rate (mm h^{-1}), $\overline{p}^o$ is the observed mean pixel rain rate (mm h^{-1}), and K is the number of pixels in the grid. Equation (2) can be rewritten as

$$E = [\overline{p}^o(N - R) + (\overline{p}^e - \overline{p}^o)N]/K. \tag{3}$$

In Eq. (3), the quantity $(N - R)$ represents the error in estimating the rain area, and it is exclusively determined by the selection of an IR temperature threshold that determines the number of estimated rain pixels N. Similarly, $(\overline{p}^e - \overline{p}^o)$ represents the error in estimating the mean rain rate, which is determined primarily by the estimated mean pixel rain rate. Besides their magnitudes, the signs of the two terms affect the total estimation error. In other words, they can compensate for each other when they have opposite signs. Of course, a mechanism that allows for error reduction through a controlled compensation effect would be highly desirable. The complexities of cloud systems cause N and $\overline{p}^o$ to be random, and thus make the utilization of such a compensation effect practically impossible. If observed values of R and $\overline{p}^o$ are available, then the proper selection of ideal values of the mean rain rate $\overline{p}^e$ and the IR threshold parameter T can diminish both error terms. However, because of the lack of sufficient ground rainfall observations, our ability to estimate such ideal parameters is severely limited for most of the earth's surface, especially over vast oceanic areas. Fortunately, microwave observations from polar-orbiting satellites can be used to reveal these ideal parameters through a series of sparsely discrete ''glimpses,'' from which an approximately ''whole picture'' can be constructed.

By calibrating the two GPI parameters to reduce total error between IR-based and microwave-based precipitation estimates, the sparse, but superior, microwave-based estimates are used to provide the standard to which GPI can be calibrated. To estimate the values of the ideal parameters using microwave observations, we first rewrite the optimization of Eq. (3) as follows:

$$(T^*, \overline{p}^*) = \min_{T,\overline{p}} |E(T, \overline{p})| = \min_{T,\overline{p}} |\overline{p}_M[N_M(T) - R_M] + (\overline{p} - \overline{p}_M)N_M(T)|, \tag{4}$$

where $(T^*, \overline{p}^*)$ are optimal estimates of the ideal parameters for a given month, R_M is the monthly summation of microwave-observed rain pixels for a grid, $N_M(T)$ is the number of IR-estimated rain pixels defined by temperature threshold parameter T and accumulated over the microwave-sampling periods in a month, and $\overline{p}_M$ is the mean microwave estimated rain rate. Notice that K does not appear in Eq. (4) because there is a constant number of pixels within each grid. The second term of the right-hand side of Eq. (4) vanishes when $\overline{p}_M = \overline{p}$, and the optimization problem becomes

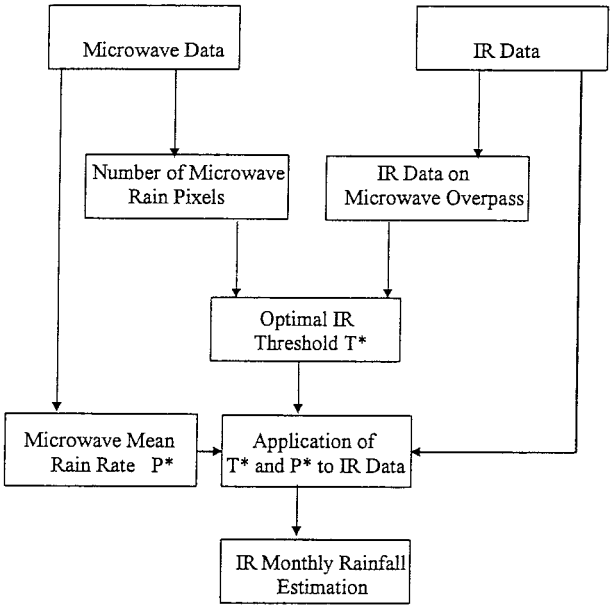

FIG. 1. A schematic diagram for illustrating the application of the UAGPI method for monthly rainfall estimation.

$$T^* = \min_T |N_M(T) - R_M| \tag{5}$$

and

$$\overline{p}^* = \overline{p}_M. \tag{6}$$

Obviously, $\overline{p}_M$ is derived directly from the microwave observations, and T^* is a product of combining microwave and IR data. It is important to mention that, so far, each grid is treated independently and has its own optimal parameters. In essence, UAGPI forces the number of IR-estimated rain pixels to approach that of ground-observed, or microwave-observed, rain pixels over a month-long period. This is achieved by adjusting the IR temperature threshold parameter using observed or microwave rainfall. A procedure to apply UAGPI for rainfall estimation is schematically outlined in Fig. 1 and summarized below:

1) calculate R_M and $\overline{p}_M$ from microwave data,
2) determine the optimal IR temperature threshold (T^*) through Eq. (5),
3) compute cold cloud fractional coverage F_C defined by T^*: $F_C = N_M(T^*)/K$, and
4) multiply F_C and $\overline{p}_M$ to produce hourly rainfall estimates and cumulate them to obtain monthly rainfall estimates.

4. Application and comparison with AGPI

Techniques to combine microwave and IR data are generally designed to first establish an IR–microwave relationship during the microwave sampling periods and then to extend this relationship to the entire month. To appropriately evaluate the performance of these methods, two error sources that are associated with the microwave technique need to be addressed. First, there are measurement errors of instantaneous rainfall, which are related to the quality of the microwave technique. Second, there are sampling errors caused by the low frequency of coverage of microwave observations, which represent the deficiency of the microwave temporal sampling rate in estimating monthly rainfall totals. Both types of errors, especially the latter, have not been well studied. The effectiveness of AGPI and UAGPI will depend on how each method tends to propagate the two types of error into uncertainty in rainfall estimates. In this section, we address the two types of error and compare UAGPI and AGPI performances using the first AIP/1 dataset.

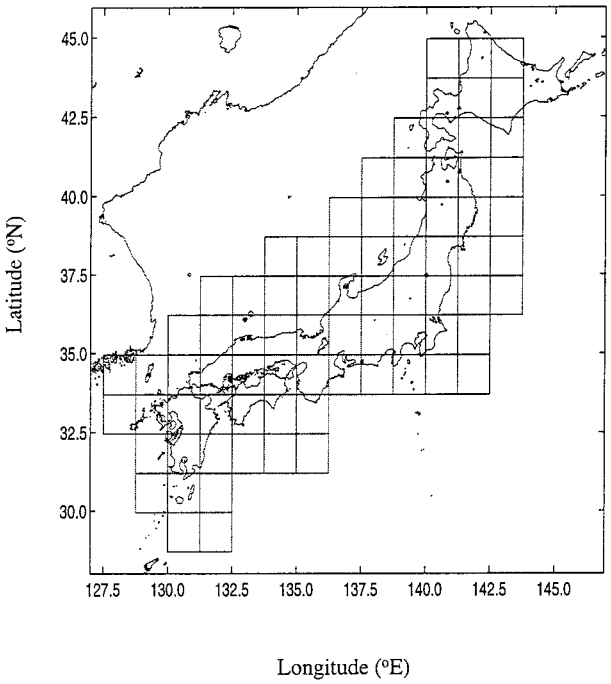

FIG. 2. The study area, which includes the Japanese islands and adjacent oceanic regions.

a. AIP/1 dataset

AIP/1 was initiated by the World Climate Research Program's GPCP to assess the skills of various algorithms of rainfall estimation using satellite observations. As seen in Fig. 2, the study area of AIP/1 encompasses the Japanese islands and the surrounding oceanic regions. The dataset includes two month-long periods in 1989: 1–30 June (hereafter referred to as the June dataset) and 15 July–15 August (hereafter referred to as the July/August dataset). The selection of these periods enabled the investigation of two rainfall regimes typical to the region: a persistent bai-u frontal regime (June) and a subtropical convective regime (July/August). A ground precipitation dataset in the form of radar–gauge

composite was assembled by the Japanese Meteorological Agency through radar and high-density rain gauge networks. Satellite data included IR images from the Japanese Geostationary Meteorological Satellite and multichannel microwave images from the SSM/I instruments aboard the Defense Meteorological Satellite Program series of sun-synchronous, polar-orbiting platforms. Both ground rainfall and IR imagery were hourly data, while SSM/I observations covered the study area at an average twice-a-day frequency. In the following analysis, AIP/1, GMS, and SSM/I datasets (originally at $0.05^\circ \times 0.0625^\circ$ pixel resolution) were reprocessed to produce $1.25^\circ \times 1.25^\circ$ climatological grids consisting of 25 pixels of $0.25^\circ \times 0.25^\circ$ each. The $1.25^\circ \times 1.25^\circ$ grid scale was selected to maintain consistency with the AIP/1 study. More details about the AIP/1 dataset can be found in Lee et al. (1991). Finally, in the research presented herein, a distinction between rain and no-rain pixels was achieved by considering a 0.25 mm h^{-1} rain-rate threshold applied radar–rain gauge composite.

b. Effects of sampling frequency errors

As mentioned before, there are two types of errors associated with using microwave-based monthly rainfall estimation. Of these uncertainties, measurement errors, which are associated with factors such as the complexity of cloud structure, ground interference, and the heterogeneity of vegetation and surface roughness, are yet to be understood effectively (Ferraro and Marks 1995). Their presence impedes the accurate assessment of the effects of sampling frequency errors on the performance of microwave-based adjustments of GPI. Consequently, the SSM/I data, which contain substantial error in measuring instantaneous rain rate (Ferraro and Marks 1995), are not suitable in evaluating the ability of AGPI and UAGPI to overcome the sampling-rate deficiency. To obtain measurement-error-free rainfall data, API/1 radar–gauge composites were used to simulate microwave rain-rate estimates. This was achieved by extracting swathlike rain-rate images from these composites so that each image corresponds both in time and in space to an actual SSM/I overpass. The resulting dataset will be referred to as the radar-simulated microwave rainfall (RSMR).

Similar to the definition of sampling error for microwave techniques, the sampling error associated with AGPI or UAGPI is the estimation error when RSMR data are combined with IR data to produce adjusted GPI monthly rainfall estimates. The adjustment ratio of AGPI defined in Eq. (1) can be rewritten as

$$r_a = \frac{\overline{p}_M R_M}{3N_M}, \tag{7}$$

where R_M is the number of rain pixels calculated using RSMR data over a month, $\overline{p}_M$ is the mean rain rate obtained from RSMR data, and N_M is the number of estimated rain pixels defined by GPI threshold using the IR data matched with SSM/I overpasses. The monthly rainfall estimate by AGPI using the RSMR data is

$$V_{\text{AGPI}} = r_a(3N_G) = \overline{p}_M\left(\frac{R_M}{N_M}N_G\right) = \overline{p}_M N_A, \tag{8}$$

where N_G is the number of estimated rain pixels by GPI threshold using the full IR data over a month, and

$$N_A = \frac{R_M}{N_M}N_G. \tag{9}$$

Although N_A takes the place of the number of rain pixels in Eq. (8), it is not the actual number of estimated rain pixels. Indeed, it is only equivalent to the real number when the final value of monthly rainfall estimation is considered. In essence, the AGPI adjustment ratio does not modify the estimated rain area limited by N_G. Rather, it adjusts the mean rain rate by an ''effective'' ratio α_M:

$$\alpha_M = \frac{R_M}{N_M}. \tag{10}$$

However, defining the ''equivalent'' number of estimated rain pixels simplifies the comparison of AGPI and UAGPI with respect to sampling errors. If R denotes the number of rain pixels and $\overline{p}^o$ denotes the mean rain rate derived from the full ground-observed rainfall data, then the error of monthly rainfall estimation by AGPI is

$$\begin{aligned} E_{\text{AGPI}} &= \overline{p}_M N_A - \overline{p}^o R, \\ &= (\delta\overline{p}_M + \delta N_A + \delta\overline{p}_M \delta N_A)\overline{p}^o R, \\ &= E(p) + E(N_A) + \frac{E(p)E(N_A)}{\overline{p}^o R}, \end{aligned} \tag{11}$$

where δ denotes the operator of relative error, that is,

$$\delta\overline{p}_M = \frac{\overline{p}_M - \overline{p}^o}{\overline{p}^o}, \qquad \delta N_A = \frac{N_A - R}{R},$$

and

$$E(p) = \delta\overline{p}_M\overline{p}^o R \quad \text{and} \quad E(N_A) = \delta N_A \overline{p}^o R.$$

The first term in Eq. (11) represents the sampling error of $\overline{p}_M$, and the second term corresponds with the sampling error of N_A. The third term is a product of the first two terms and describes the interaction between the errors in estimating mean rain rate and the number of rain pixels. The monthly rainfall estimate by UAGPI can be expressed as

$$V_{\text{UAGPI}} = \overline{p}_M N_{T^*}, \tag{12}$$

where N_{T^*} denotes the number of cloud pixels colder than the optimal IR threshold T^* in a grid over a month-long period. Similar to the above analysis, the estimation error for UAGPI is given by

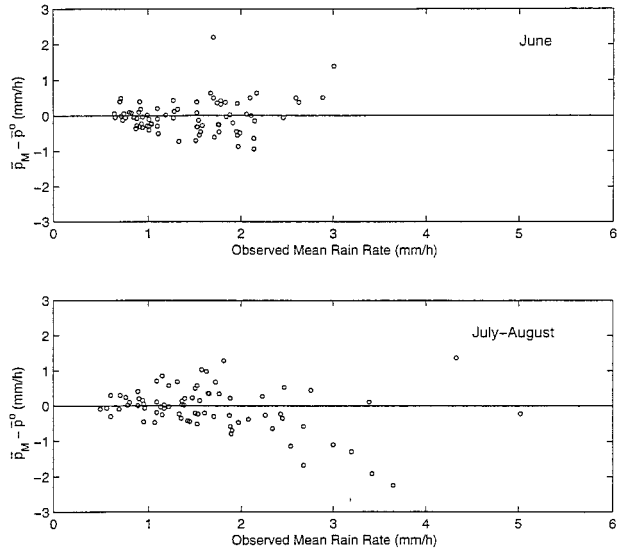

FIG. 3. Sampling error of monthly mean rain rate $\overline{p}_M$ for the 79 grids in the study area.

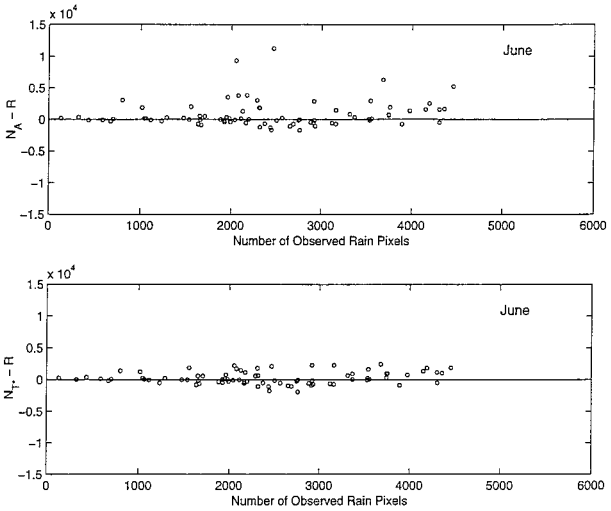

FIG. 4. Sampling error of the equivalent rain pixel number N_A for AGPI and the rain pixel number N_{T^*} for UAGPI in Jun 1989 of the Japanese region.

$$E_{\text{UAGPI}} = \overline{p}_M N_{T^*} - \overline{p}^o R,$$
$$= (\delta\overline{p}_M + \delta N_{T^*} + \delta\overline{p}_M \delta N_{T^*})\overline{p}^o R,$$
$$= E(p) + E(N_{T^*}) + \frac{E(p)E(N_{T^*})}{\overline{p}^o R}, \qquad (13)$$

where $\delta\overline{p}_M$ and $E(p)$ have the same meaning as in Eq. (11), and

$$\delta N_{T^*} = \frac{N_{T^*} - R}{R}$$

and

$$E(N_{T^*}) = \delta N_{T^*}\overline{p}^o R.$$

Comparing Eqs. (11) and (13), the only difference in sampling errors of AGPI and UAGPI methods rests on the distinction between an ''equivalent'' number of estimated rain pixels and the number of rain pixels defined by the optimal IR threshold. The total error is not only affected by the errors in estimating the number of rain pixels and mean rate but also by their interactions, including their signs. The interaction, however, is highly random due to the complexity of clouds. Arguably, more insight can be gained by examining the effects of sampling frequency on the magnitudes of the errors in estimating $\overline{p}_M$, N_A, and N_{T^*} than by examining the total estimation error.

Root mean square error (rmse) was used to quantify the magnitudes of sampling errors for the above-mentioned quantities. Because RSMR snapshots were selected to match SSM/I scenes, the resulting rmse values are determined by the low sampling rate of the SSM/I coverage. The distributions of the sampling errors in $\overline{p}_M$ are presented in Fig. 3, and those corresponding to N_A and N_{T^*} are presented in Fig. 4 for the June dataset and in Fig. 5 for the July–August dataset. For each grid, sampling errors were computed by subtracting the estimated values from their observed counterparts. In Fig. 3, the noticeably wider range of errors associated with the July–August period can be attributed to the convective storms common during this period, as opposed to the large-scale bai-u frontal systems in June. This indicates that microwave-based measurements of mean rain rates during convective rainfall regimes require higher sampling frequencies than those necessary to describe large-scale frontal systems.

A summary of the rmse associated with $\overline{p}_M$, N_A, and N_{T^*} is provided in Table 1. From Table 1, as well as from Figs. 4 and 5, it is clear that UAGPI-based esti-

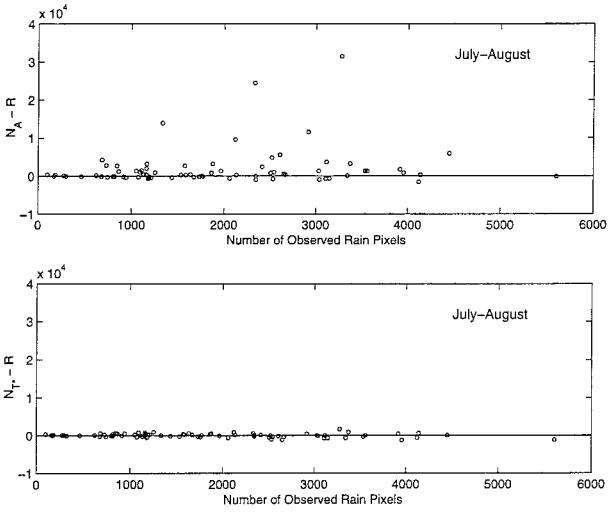

FIG. 5. Sampling error of the equivalent rain pixel number N_A for AGPI and the rain pixel number N_{T^*} for UAGPI in Jul–Aug 1989 of the Japanese region.

TABLE 1. Root-mean-square errors for estimated mean rain rate and number of rain pixels using RMSR data.

rmse	Jun	Jul–Aug
p_M (mm h^{-1})	0.47	0.63
N_A (pixel)	2278	5363
N_{T^*} (pixel)	1011	504

TABLE 2. Rainfall estimation errors associated with estimated mean rain rate and number of rain pixels using RMSR data. (Units in mm.)

rms	Jun	Jul–Aug
$E(p)$	47.2	50.8
$E(N_A)$	116.8	464.0
$E(N_{T^*})$	59.2	38.9

mates of the number of rain pixels are superior to those associated with AGPI. The rmse and bias of N_{T^*} are consistently smaller than those of N_A in both months, suggesting that using an optimal IR temperature threshold T^* is a more effective means of utilizing microwave data than using the AGPI adjustment ratio. It must be mentioned also that two grids were removed before computing the rmse of N_A during July–August because of zero N_M values. The inability of the GPI default temperature threshold parameter to capture warm convective precipitation resulted in AGPI's inability to compute the number of rain pixels over these two grids. This presents a limitation for AGPI applications over grids where the GPI threshold fails to define any rain pixels in a month-long period.

Although rmse values of $\overline{p}_M$, N_A, and N_{T^*} are not explicit determinants of the error in estimating the monthly rainfall by AGPI or UAGPI, they do enable the examination of the main sources of estimation error. The contributions of sampling errors in $\overline{p}_M$, N_A, and N_{T^*} to the total sampling errors of monthly rainfall were computed using Eqs. (11) and (13). The root mean square (rms) values associated with each individual contribution [i.e., $E(N_A)$, $E(p)$, and $E(N_{T^*})$] are presented in Table 2. Clearly, UAGPI produced comparable contributions of the sampling errors in the mean rain rate and in the number of rain pixels to the total sampling error. AGPI, on the other hand, resulted in a dominant contribution of sampling errors in the number of rain pixels to the total sampling error.

c. Comparison of monthly rainfall estimates

To evaluate the accuracy of the two microwave–IR combination techniques in capturing total monthly rainfall, observed values were computed using ground-based radar–gauge composites over each grid in the study area. These values were then compared to monthly rainfall estimates obtained using RSMR, AGPI, and UAGPI. Both AGPI and UAGPI were applied to the combination of IR and RSMR data described above, and the RSMR monthly estimates were obtained through linear extension of the RSMR's snapshots to cover the entire month. A comparison between observed and estimated monthly rainfall is provided in Fig. 6, and a statistical summary of estimation error is provided in Table 3.

Despite the fact that using RSMR data makes the UAGPI and AGPI estimates more closely resemble the radar–gauge observations, AGPI displayed a poorer performance in monthly rainfall estimation than that by UAGPI as well as that by the linear extension of the RSMR data. As seen in Fig. 6 and Table 3, bias and rmse values of AGPI are consistently higher than those corresponding to UAGPI and RSMR. In fact, AGPI shows a strong tendency toward overestimation during both the June and July–August periods. In both cases, the presence of many extreme points on the scatterplots corresponds to the effects of sampling frequency on N_A estimates, as shown previously in Figs. 4 and 5. The amplification of this effect during the July–August period causes AGPI to be less reliable during months with convective precipitation. On the other hand, the consistently superior performance of UAGPI in both periods suggests that the optimal IR threshold reflects properly the cloud climatology for the persistent bai-u frontal and the subtropical convective systems at AIP/1

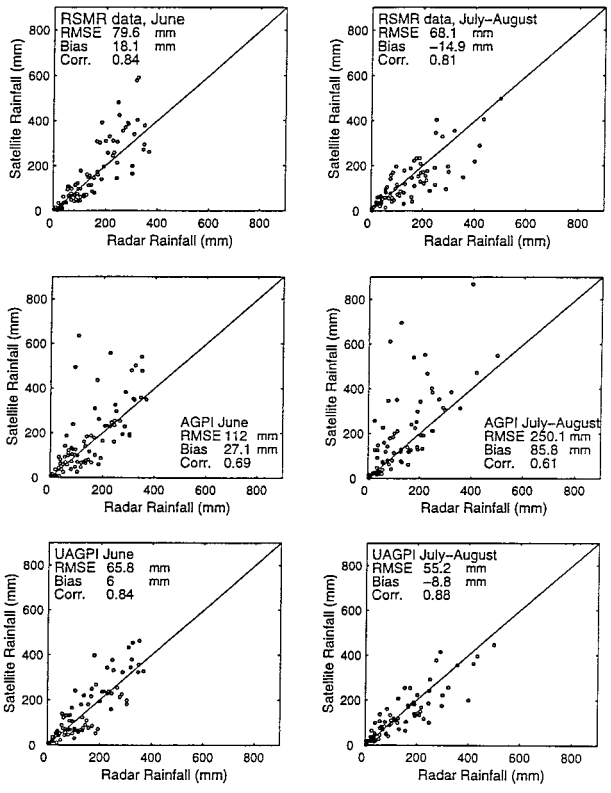

FIG. 6. Monthly rainfall estimates by RSMR data, AGPI, and UAGPI using radar-simulated microwave rainfall data without applying moving-average procedure in Jun and Jul–Aug 1989 of the Japanese region.

TABLE 3. Summary of statistics for monthly rainfall without applying moving-average procedure in Jun or Jul–Aug.

	Jun			Jul–Aug		
Procedure	SI	AGPI	UAGPI	SI	AGPI	UAGPI
rmse (mm)	79.6	112	65.8	68.1	250	55.2
Bias (mm)	18	27	6	−15	86	−9
Correlation	0.84	0.69	0.84	0.81	0.61	0.88

grid scales. The better performance of UAGPI over that of the linearly extended RSMR data demonstrates that UAGPI reduces the errors associated with sparse sampling and, therefore, enhances the accuracy of estimated rainfall.

d. Effects of spatial smoothing

Adler et al. (1993; 1994) proposed the application of a moving-average smoother combined with value constraints on the AGPI adjustment ratio. The purpose of the smoothing process is to compensate for the weak connection between the adjustment ratio and GPI rainfall estimates at grid scale. The objective of the constraints is to limit the large variability in the computed adjustment ratio. The moving-average smoother (Adler et al. 1993) replaces a quantity at a grid with the mean value of the quantity over a neighborhood of adjacent grids surrounding it. A 5×5 grid box was used as the moving window in the AIP/1 region for the study of AGPI (Adler et al. 1993). The moving average reduces the spatial variance of the smoothed quantity to the extent determined by the size of the selected moving window. In Fig. 7, the effects of window size on the $\overline{p}_M$, N_A, and N_{T^*} are examined. The results in Fig. 7 were obtained by computing these three quantities with moving windows varying from a single grid square to 3×3 and 5×5 grid boxes. While marginal improvements of $\overline{p}_M$ and N_{T^*} sampling errors were obtained as the size of the moving window increased from 1×1 to 3×3, a substantial reduction of sampling error in N_A was achieved. However, at the 5×5 window, the rmse values of the three quantities increased slightly. Corresponding monthly rainfall estimates are presented in Figs. 8 and 9, and their statistics are shown in Tables 4 and 5. Comparison between Figs. 6 and 8 shows that the improvements for AGPI are dramatic for both months when a moving-average window size of 3×3 is applied, and that marginal variations are demonstrated for the results of UAGPI. In addition, the extreme points

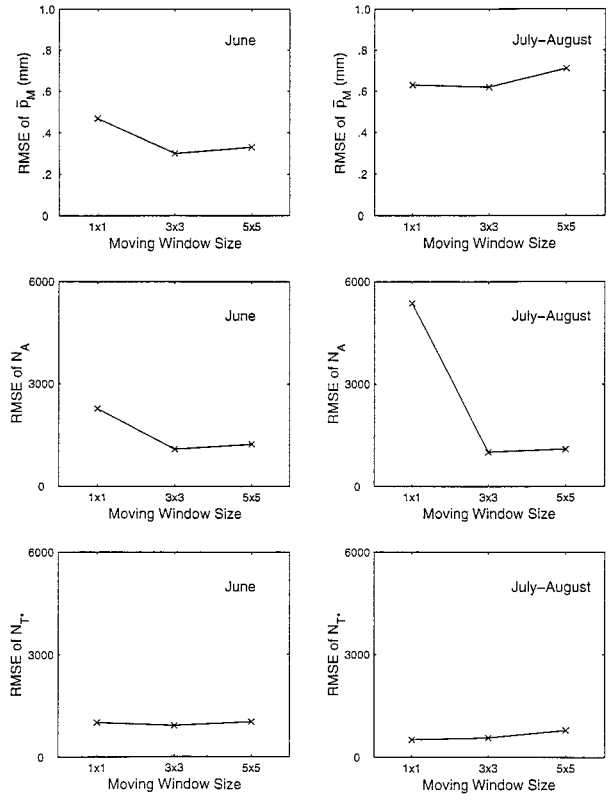

FIG. 7. Variations of rmse for the mean rain rate $\overline{p}_M$, the equivalent rain pixel number N_A for AGPI, and the rain pixel number N_{T^*} for UAGPI with change of moving-window size, using radar-simulated microwave rainfall data.

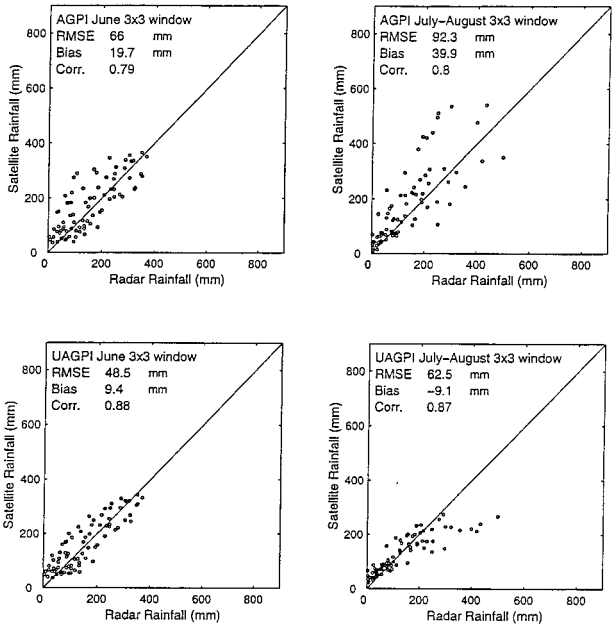

FIG. 8. Monthly rainfall estimates by AGPI and UAGPI using radar-simulated microwave rainfall data with 3×3 moving window in Jun and Jul–Aug 1989 of the Japanese region.

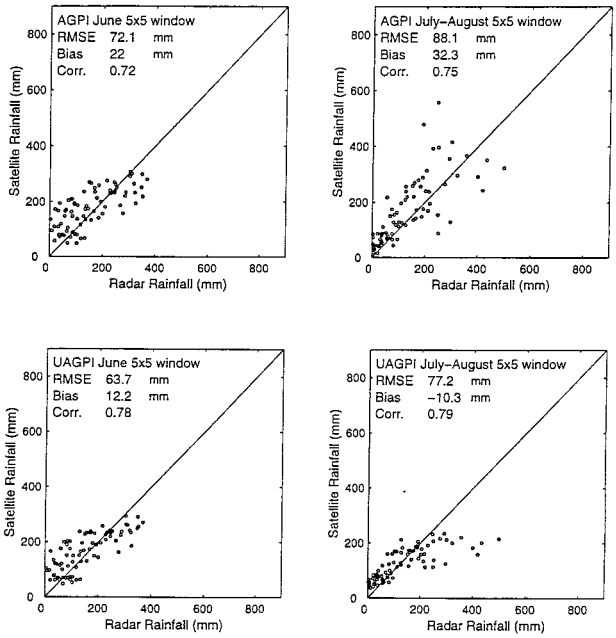

FIG. 9. Monthly rainfall estimates by AGPI and UAGPI using radar-simulated microwave rainfall data with 5 × 5 moving window in Jun and Jul–Aug 1989 of the Japanese region.

shown in Fig. 6 now behave much more reasonably after smoothing. The above result suggests that the sparse samples of microwave rain pixels within a 1.25° × 1.25° grid square provide insufficient information to derive a stable adjustment ratio in these grid squares for AGPI. By enlarging the window size, more spatially correlated rain pixels can be included in the calculation of the ratio. The seemingly auxiliary smoothing procedure turns out to be critical to the AGPI method.

e. Effects of microwave measurement errors

Measurement errors associated with microwave estimation of instantaneous rain rate affect the accuracy of microwave–IR combination techniques. To examine such effects on AGPI and UAGPI, monthly rainfall estimates were obtained by applying UAGPI and AGPI in conjunction with rainfall data estimated from the actual SSM/I imagery using the SI technique. The impacts of measurement errors on SI have been studied extensively using the AIP/1 dataset (Ferraro and Marks 1995). In general, these uncertainties are quite significant, especially over coastal areas. Therefore, an extended coastline was excluded from the study area before applying the SI method. The results of monthly rainfall estimation for 5 × 5 windows, depicted in Fig. 10, indicate that in June, both the AGPI and UAGPI methods significantly improved monthly rainfall estimates in comparison to those of GPI. Such improvement was not observed with respect to AGPI during July–August. In fact, while UAGPI continued to be superior to GPI with respect to rsme and bias, AGPI estimates were less accurate than GPI's during this period. Clearly, AGPI is more sensitive to the combined effects of sampling frequency errors and microwave measurement errors than UAGPI. However, by comparing Fig. 9 with Fig. 10, the substantial increase in rmse and bias in AGPI and

TABLE 4. Summary of statistics for monthly rainfall applying moving-average procedure in Jun and Jul–Aug for AGPI.

	Jun		Jul–Aug	
Window size	3 × 3	5 × 5	3 × 3	5 × 5
rmse (mm)	66.9	73.1	93.5	89.3
Bias (mm)	20	22	40	32
Correlation	0.79	0.72	0.8	0.75

TABLE 5. Summary of statistics for monthly rainfall applying moving-average procedure in Jun and Jul–Aug for UAGPI.

	Jun		Jul–Aug	
Window size	3 × 3	5 × 5	3 × 3	5 × 5
rmse (mm)	55.4	64.5	75.3	78.2
Bias (mm)	10	12	−8	−10
Correlation	0.84	0.78	0.78	0.79

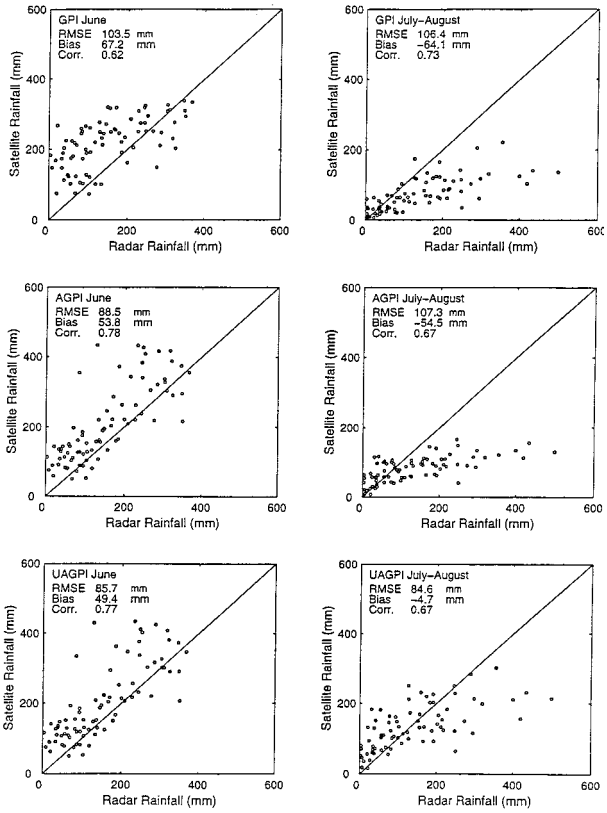

FIG. 10. Monthly rainfall estimates by AGPI and UAGPI using the actual microwave data with 5 × 5 moving window in Jun and Jul–Aug 1989 of the Japanese region.

UAGPI and the reduction of their correlation coefficients indicate that effects of measurement errors are quite substantial.

5. Summary and conclusions

Dividing rainfall estimation errors into rain area estimation errors and mean rain-rate estimation errors enables the examination of the effects of GPI parameters (i.e., the IR temperature threshold and the mean rain rate) on the accuracy of rainfall estimates. Further advances in climate studies will require the reduction of uncertainty in rainfall estimates, particularly at scales feasible to most climate models. While the two types of errors reflect uncertainties resulting from the complexities of cloud structures, they are also related closely to rainfall intensity and rain coverage area, which are important variables for most modern climate models. Clearly, detailed analysis of these errors corresponding to various techniques will provide useful insights about potential areas of improvements on such techniques.

Based on the error analysis using the AIP/1 dataset, a new method, the UAGPI, was developed. The method uses microwave rainfall data to determine optimal estimates of the two GPI parameters. In this paper, UAGPI was examined extensively using RSMR data in comparison to AGPI. Employing RSMR data is demanded by the fundamental purpose of developing techniques to combine microwave data and geosynchronous IR observations. That is, smoothing the sampling gap of microwave measurements using IR data and utilizing the superior estimates of instantaneous rain rate obtained using microwave data. As a result, sampling frequency errors and measurement errors must be addressed to understand the potentials for improving microwave–IR combination methods. Using RSMR data derived from the AIP/1 dataset, we demonstrated that the UAGPI method consistently performed better than the AGPI technique during two study periods. Furthermore, while the application of low-pass moving-average filter remains crucial to AGPI, its impact on UAGPI is marginal. This suggests that the proposed UAGPI is capable of providing better rainfall estimates for higher spatial and temporal resolutions.

Despite the large contributions of microwave measurement errors to the total error in estimating monthly rainfall, results obtained using actual SSM/I data in conjunction with both AGPI and UAGPI showed that, during the June period, both methods improved GPI monthly rainfall estimates. On the other hand, during the July–August period only UAGPI resulted in improving GPI monthly rainfall estimates. Arguably, UAGPI has the lesser tendency to amplify the impact of microwave measurement errors. More important, these results demonstrated that measurement errors associated with microwave techniques dominate the rainfall estimation errors associated with combination techniques like AGPI and UAGPI. Reducing microwave measurement error of instantaneous rainfall rate is a very crucial element of successful implementation of any combination method.

The successful launch and deployment of the TRMM satellite on 28 November 1997 initiates a new era for satellite-based precipitation estimation. TRMM will provide a great amount of satellite data, including IR, microwave, and radar data, over the entire tropical region. Notwithstanding the significant benefits generated from TRMM's higher-resolution tropical rainfall products, TRMM data can be used to further improve the accuracy of current satellite-based precipitation estimation techniques and to provide the framework for the development of future generation methods. UAGPI method is well suited to utilize TRMM data to obtain seasonally variable and regionally variable optimal parameters for GPI over the tropical regions, which plays a significant role in global weather and climate variability.

Finally, our UAGPI will soon be included in our precipitation-dedicated ''PERSIANN'' Web site available online at http://www.hwr.arizona.edu/persiann/. We invite other groups actively working on this topic to evaluate the various algorithms included in our PERSIANN system and welcome feedback and potential cooperation.

Acknowledgments. The authors would like to gratefully acknowledge the support provided by NASA's EOS-IDS Grant NASA NAG5-3640 and NOAA Pan-American Climate Studies Grant NA56-GPO-185. The senior author wishes to acknowledge the support of the Salt River Project graduate fellowship program for providing financial support during the academic years 1993 and 1994. In addition, the authors wish to extend their gratitude to Dr. Kuo-lin Hsu for his valuable discussion and review of this manuscript, and to Ms. Corrie Thies for her assistance in proofreading the manuscript.

REFERENCES

Adler, R. F., A. J. Negri, P. R. Keehn, and I. M. Hakkarinen, 1993: Estimation of monthly rainfall over Japan and surrounding waters from a combination of low-orbit microwave and geosynchronous IR data. *J. Appl. Meteor.*, **32,** 335–356.

——, G. J. Huffman, and P. R. Keehn, 1994: Global rain estimates from microwave adjusted geosynchronous IR data. *Remote Sens. Rev.*, **11,** 125–152.

Arkin, P. A., 1979: The relationship between fractional coverage of high cloud and rainfall accumulations during GATE over the B-scale array. *Mon. Wea. Rev.*, **107,** 1382–1387.

——, and B. N. Meisner, 1987: The relationship between large-scale convective rainfall and cold cloud over the Western Hemisphere during 1982–84. *Mon. Wea. Rev.*, **115,** 51–74.

——, and P. E. Ardanuy, 1989: Estimating climatic-scale precipitation from space: A review. *J. Climate*, **2,** 1229–1238.

——, and P. Xie, 1994: The global precipitation climatology project: First algorithm intercomparison project. *Bull. Amer. Meteor. Soc.*, **75,** 401–419.

Ebert, E. E., M. J. Manton, P. A. Arkin, R. J. Allam, G. E. Holpin,

and A. Gruber, 1996: Results from the GPCP algorithm intercomparison program. *Bull. Amer. Meteor. Soc.,* **77,** 2875–2886.

Ferraro, R. R., and G. F. Marks, 1995: The development of SSM/I rain-rate retrieval algorithms using ground-based radar measurements. *J. Atmos. Oceanic Technol.,* **12,** 775–770.

Grody, N. C., 1991: Classification of snow cover and precipitation using the Special Sensor Microwave Imager. *J. Geophys. Res.,* **96,** 7423–7435.

Hsu, K., X. Gao, S. Sorooshian, and H. V. Gupta, 1997: Precipitation estimation from remotely sensed information using artificial neural networks. *J. Appl. Meteor.,* **36,** 1176–1190.

Huffman, G. J., and Coauthors, 1997: The Global Precipitation Climatology Project (GPCP) combined precipitation dataset. *Bull. Amer. Meteor. Soc.,* **78,** 5–20.

Lee, T. H., J. E. Janowiak, and P. A. Arkin, 1991: *Atlas of Products from the Algorithm Intercomparison Project 1: Japan and Surrounding Oceanic Regions June–August 1989.* University Corporation for Atmospheric Research, 131 pp.

Morrissey, M. L., and J.S. Greene, 1993: Comparison of two satellite-based rainfall algorithms using Pacific atoll raingage data. *J. Appl. Meteor*, **32,** 411–425.

Simpson, J., R. F. Adler, and G. R. North, 1988: A proposed tropical rainfall measuring mission. *Bull. Amer. Meteor. Soc.,* **69,** 278–295.

Sorooshian, S., 1997: Precipitation estimation from remotely sensed information using artificial neural network model. *GEWEX News,* **7,** (2).

Xie, P., and P. A. Arkin, 1996: Analysis of global monthly precipitation using gauge observations, satellite estimates, and numerical model predictions. *J. Climate,* **9,** 840–858.

——, and ——, 1997: Global precipitation: A 17-year monthly analysis based on gauge observations, satellite estimates, and numerical model outputs. *Bull. Amer. Meteor. Soc.,* **78,** 2539–2558.

Xu, L., 1997: Estimating rainfall from satellite infrared imagery: Cloud patch analysis. Ph.D. dissertation, The University of Arizona, 198 pp. [Available from Main Library, University of Arizona, Tucson, AZ 85721-0055.]